FABRICATION AND CHARACTERIZATION OF RESONANT CAVITY LIGHT-EMITTING TRANSISTORS

BY

MICHAEL E. LIU

THESIS

Submitted in partial fulfillment of the requirements
for the degree of Master of Science in Electrical and Computer Engineering
in the Graduate College of the
University of Illinois at Urbana-Champaign, 2013

Urbana, Illinois

Adviser:

Professor Milton Feng

Abstract

The development of optical interconnects and optical communication has enabled high-speed, energy-efficient and reliable data transmission in supercomputers and communication networks. Nowadays, with the improvement in computer processing speed, higher data transmission rate is required to enhance the overall performance of electronics. Light-emitting transistors (LETs) are attractive optical signal sources because of their inherent dynamic charge transport mechanism in the base terminal. LETs have demonstrated GHz modulation capability, and in order to further improve the emission intensity and spectral purity, resonant cavity is introduced into the LET structure. Resonant cavity light-emitting transistors (RCLETs) have demonstrated up to 68% enhancement in the peak emission intensity and narrower emission peak compared with conventional LETs. The work described in this thesis involves the fabrication process and device characterization of the RCLETs.

To my family, for love and support

Acknowledgments

I would like to thank my adviser, Professor Milton Feng, for his support and guidance. The training and advice I have received from him are invaluable. My mentor, Mong-Kai Wu, has not only taught me the fabrication process but also shown me how to be productive in research. All the experimental skills, tips, knowledge, and, most importantly, attitude I have learned from him make me realize how little I know and how much more I need to learn and improve in order to produce competitive research results. I am thankful for such a great mentor.

HSIC group members Rohan Bambery, Eric Iverson, Fei Tan, and Huiming Xu have all helped me in research with great advice and answers to my questions. I am lucky to be in this great group.

Last but not least, I would like to thank my family and friends for always being there for me and giving me lots of love and support. I am glad to have all of you in my life.

Table of Contents

Chapter 1: Introduction

Optical interconnects have been used to replace electrical interconnects in supercomputers and communication networks in order to maintain high performance. With increasing operating frequency, electrical interconnects suffer crosstalk noise from the radiating electromagnetic fields of the neighboring metallic wires. Also, the resistance-capacitance (RC) charging time of the electrical interconnects will limit the operating frequency. To achieve high data rate, optical interconnects are used because they are power-efficient and immune to the electromagnetic fields in the environment .

An attractive optical signal source, the light-emitting transistor (LET), was first proposed in 2004. Light modulation was first observed in the base terminal of a high-speed heterojunction bipolar transistor (HBT) [1]. Later in 2004, LET with quantum wells inserted in the base to enhance radiative recombination was reported with GHz operation capability [2]. In 2009, 4.3 GHz direct optical modulation bandwidth was then demonstrated [3]. In order to further enhance the emission intensity and spectral purity for optical communication applications, resonant cavity with distributed Bragg reflector (DBR) mirrors is introduced into the conventional LET structure [4].

Chapter 2: Heterojunction Bipolar Transistors

2.1 Bipolar Junction Transistors

In an n-p-n bipolar junction transistor (BJT), the emitter, the base, and the collector are made of same material but with different dopants and doping levels. Figure 1 shows the band diagram of an n-p-n BJT under forward-active operation which is emitter-base being forward biased and base-collector being reverse-biased.

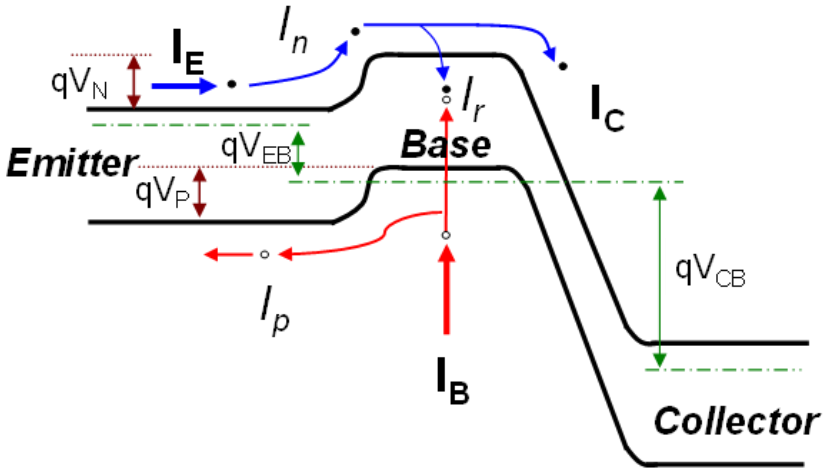

Figure 1. Band diagram of an n-p-n type bipolar junction transistor (BJT) under forward-active operation

The emitter current, I_E, injects electrons, I_n, into the p-type base. The injected electrons in the base diffuse toward the collector through the base, and some injected electrons recombine with the majority holes forming the recombination current, I_r. The electrons that do not recombine and reach the depletion region of the base-collector junction are swept to the collector by the built-in field to form the collector current, I_C. Since the base-emitter junction is forward biased, p-type base has a current component,

I_p, which injects holes into the emitter. The amplification of a bipolar transistor is defined as the current gain, β, in Equation 2.1.

$$\beta \cong \frac{I_C}{\mathrm{I}_B} = \frac{I_n - I_r}{I_r + I_p} \tag{2.1}$$

In a homostructure BJT, in order to improve β, the emitter is heavily doped for more electron injection into the base, and the base is lightly doped to minimize the hole injection current, I_p. However, a heavily doped emitter may shift the Fermi level into the conduction band and cause band gap shrinkage to lower the current gain. Also, a heavily doped emitter increases the junction capacitance and limits the modulation speed with long RC charging time. On the other hand, a lightly doped base layer leads to a more resistive base, and to lower the base resistance, a thick base is required. It takes a longer transit time, τ_t, for electrons to diffuse through a thick base layer and lowers β, which can represented in terms of transit time, τ_t, and recombination lifetime, τ_n, as in Equation 2.2. In addition, a longer transit time means a slower AC response of the collector current.

$$\beta = \frac{\tau_n}{\tau_t} \tag{2.2}$$

2.2 Heterojunction Bipolar Transistors

The idea of using wider band gap emitter to enhance a bipolar transistor was first pointed out by Shockley [5]. Later, Kroemer proposed the structure of the first heterojunction bipolar transistor, HBT, with a larger band gap emitter to prevent the hole injection from the base to the emitter [6]. Figure 2 shows the band diagram of an n-p-n

HBT in forward-active operating mode. Different from a BJT, the potential barrier, qV_P, in the valance band at the emitter-base junction is much greater because of the wider band gap emitter. With the band discontinuity at the emitter-base junction, the injection of holes from base to emitter is greatly suppressed. In an HBT case, the current gain, β, can be approximated as in Equation 2.3. With the hole injection being much suppressed, an HBT can achieve a higher current gain than a BJT.

$$\beta \cong \frac{I_C}{I_B} = \frac{I_n - I_r}{I_r} \tag{2.3}$$

Since the band discontinuity only favors electron injection, the emitter in an HBT can be lightly doped to reduce the junction capacitance for faster operation. Also, the base can be heavily doped without much penalty in the current gain. A high doping level reduces the resistivity, and a thin base layer can be used in an HBT to reduce the carrier transit time, τ_t, for higher current gain and faster ac response at the collector.

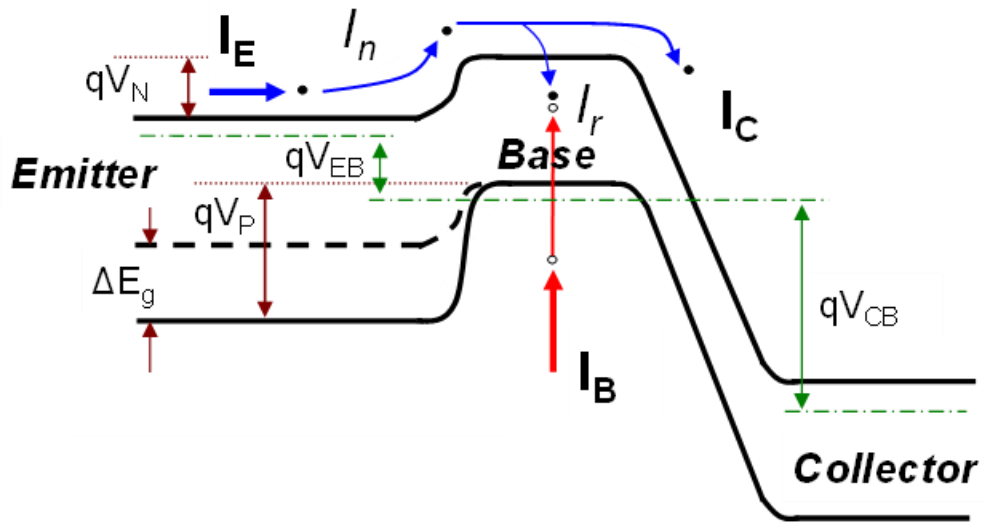

Figure 2. Band diagram of an n-p-n heterojunction bipolar transistor under forward-active operation [7]

Chapter 3: Development of Light-Emitting Transistors

3.1 Light Modulation in the Base

In an HBT, the base current is mainly made of the recombination currents because the hole injection current into the emitter is much suppressed by the large potential barrier. The surface recombination current and extrinsic recombination currents in an HBT fabricated with good ledge passivation on the exposed base area can be significantly reduced. Hall-Shockley-Read process, Auger recombination, and radiative recombination are the main recombination mechanisms in the bulk of the base. In 2004, light modulation from radiative recombination in the base of an InGaP/GaAs HBT was first reported, i.e. the first light-emitting transistor (LET). Figure 3 shows the microscopic view of optical emission from the base of the first LET captured by a silicon CCD [1].

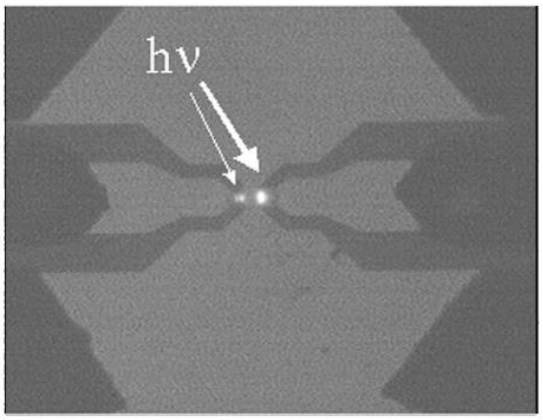

Figure 3. Optical emission from the base of an HBT under normal operating bias condition [1]

The modulation speed of the optical signal output in response to electrical input, the base current, of this device is limited at 1 MHz because the device geometry has not been optimized for optical output. However, the realization of a three-port light emitting

device, i.e. the LET, has been demonstrated. Also, an HBT's capability of high speed modulation has indicated the potential of a high-speed LET.

3.2 Quantum-Well Light-Emitting Transistors

To enhance the light emission of a light-emitting transistor, quantum wells are included in the base of an LET [2]. Quantum wells can provide carrier confinement to enhance radiative recombination in the base. Also, the emission wavelength can be engineered by variation in barrier heights and well widths. Figure 4 shows the band diagram of the quantum-well LET (QWLET). The QWLET includes an n-type InGaP wide-gap emitter, a carbon-doped p^+-GaAs base with two intrinsic InGaAs quantum wells, and an n-type GaAs collector. Two different emission wavelengths are observed, which are the band-to-band emissions from the GaAs base and InGaAs quantum wells.

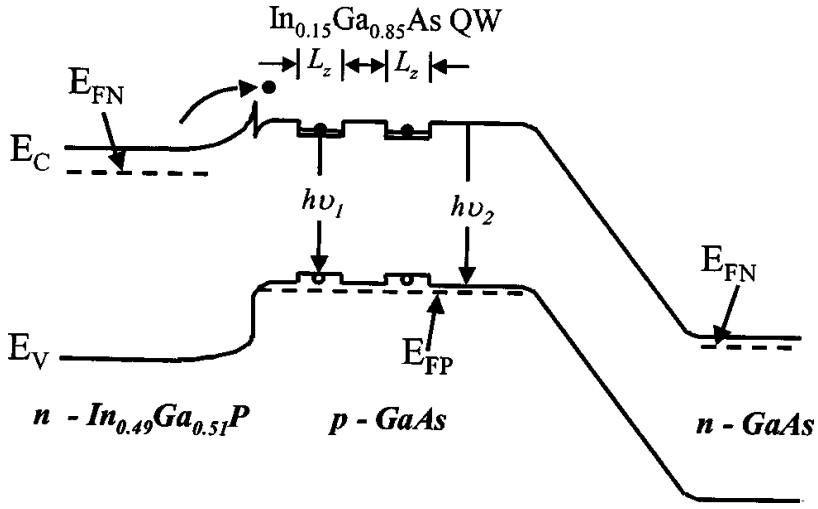

Figure 4. The band diagram of a QW InGaP/GaAs LET with two InGaAs quantum wells in the base to capture carriers and enhance radiative recombination [2]

Figure 5(a) shows the top view of the QWLET, and Figure 5(b) is the CCD image of light emission from the QWLET under forward active bias in common-emitter configuration with 1mA base current. As seen in Fig. 5(b), the light emission is in the emitter-base region but not the base-collector junction because electrons near the base-collector junction are swept to collector by the built-in field and do not have the time to recombine [2].

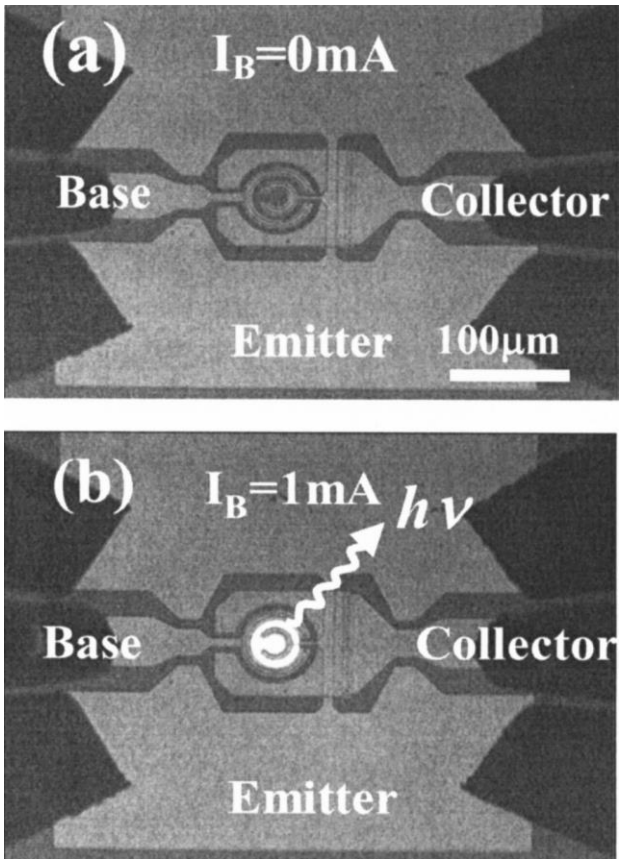

Figure 5. (a) Top view of the QWLET with 45-μm diameter light-emitting area, and (b) light emission of QWLET under 1mA base current in common-emitter configuration captured by silicon CCD detector [2]

To test the modulation speed of a QWLET, a pattern generator is used as the electrical input signal source at the base terminal. Figure 6 shows the (a) electrical input,

(b) electrical output, and (c) optical output of a QWLET on an oscilloscope with 1 GHz electrical input signal. The electrical output is taken at the collector, and the emission light is coupled into a multimode fiber probe and fed into a photodetector. As seen in Figure 6(c), the optical output can be modulated at 1 GHz. With quantum wells in the base, the radiative recombination is enhanced, and GHz optical response in a three-port QWLET is demonstrated.

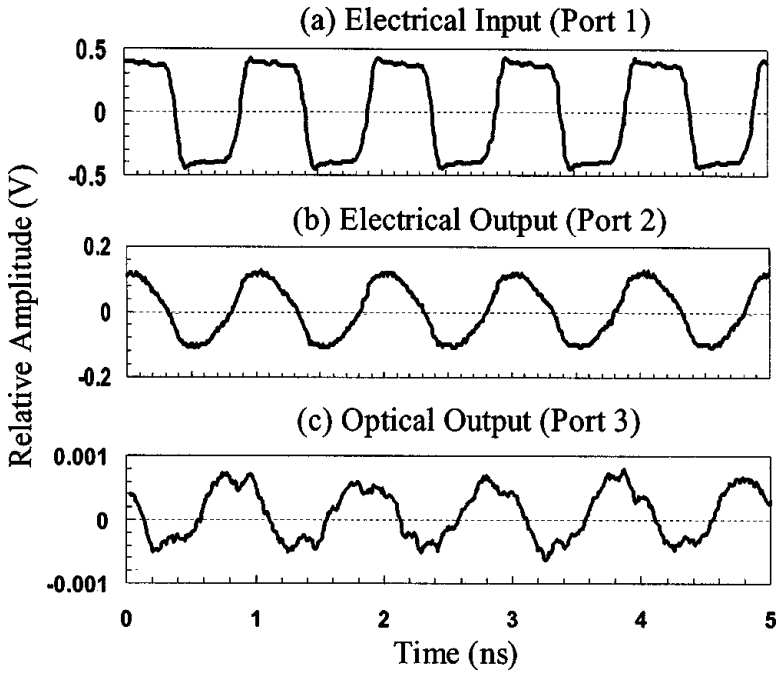

Figure 6. The signals in ac operation of a QWLET shown on an oscilloscope (a) a 1GHz electrical input signal from pattern generator fed into the base, (b) electrical output taken at the collector, and (c) the optical output modulated at 1GHz [2]

3.3 Light-Emitting Diodes and Light-Emitting Transistors

The operation speed of a reliable light-emitting diode (LED) for communication purposes is limited to a modulation speed below 1 GHz due to the minority carrier

lifetime in the active region. The fastest reported LED has a modulation speed of 1.7 GHz achieved by a high doping level in the active region [8]. Although a heavily doped active region can reduce the radiative recombination lifetime for faster optical response, the non-radiative recombination mechanisms are also enhanced; thus, the luminescence efficiency is decreased due to impurity scattering and recombination at the defects.

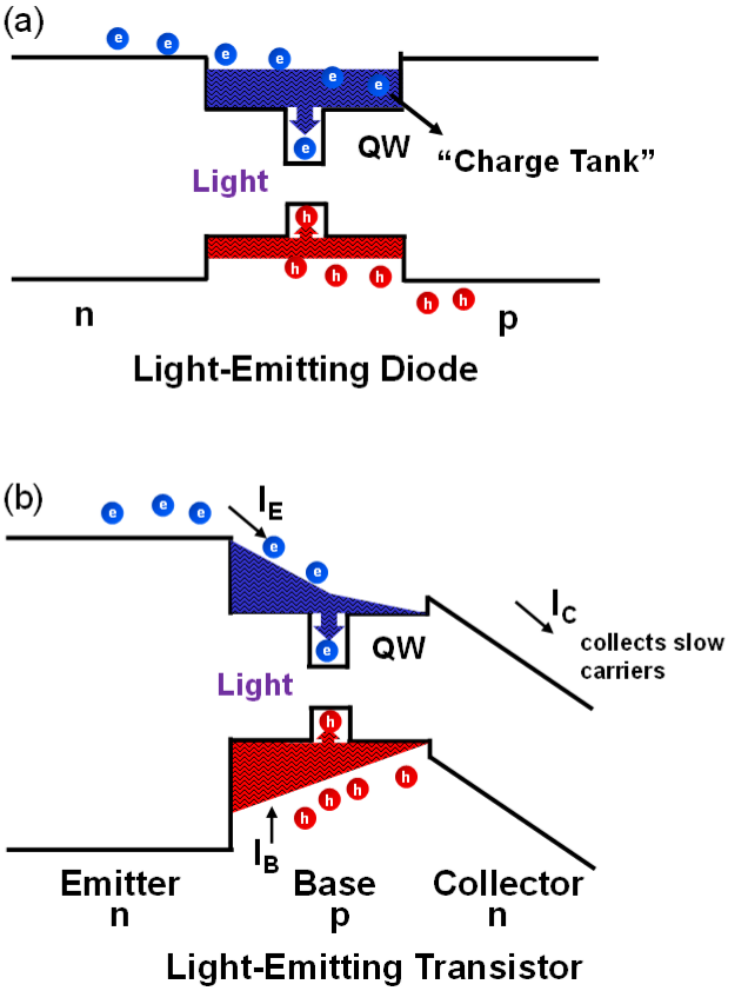

Figure 7. (a) Band diagram and carrier distribution in the active region of a p-i-n structure LED, and (b) band diagram and the tilted charge distribution in the base of an n-p-n LET

Figure 7 (a) shows the band diagram and the carrier distribution in the active region of a conventional p-i-n LED. The n and p-terminals inject carriers into the active region, and the active region acts like a charge tank and contains a large number of carriers. Carriers wait to recombine in the quantum well while an LED is being modulated, and due to the large density of carriers in the active region, the speed of optical response is limited. In a diode structure, the carrier recombination lifetime for spontaneous emission is about 1 nanosecond, which limits the optical response to less than 1 GHz.

The carrier distribution in the base of an n-p-n LET is shown in Figure 7(b). The electrons are injected from the emitter, and the holes are provided by the base current. The minority electrons have the highest concentration at the edge of the emitter-base junction, so the carrier distribution shows a tilted profile, and the charge distribution of the majority holes is also tilted to maintain charge neutrality. The injected electrons will diffuse toward collector based on the concentration gradient. While diffusing through the base, the carriers pass the quantum-well active region, and if they cannot recombine fast enough in the quantum well, those electrons are swept to the collector by the large built-in field and the base-collector junction. "Fast" mentioned in the previous sentence does not refer to the actual speed of a carrier's motion; rather, it means a carrier can recombine radiatively in a shorter time than it takes to diffuse across the base, i.e. the transit time, τ_t. In a three-port LET, because of the collector, the carriers that do not recombine radiatively in the quantum well within the base transit time are swept to collector and form collector current. In a typical LET, the base transit time is about few picoseconds

[3]; thus, in contrast to the LED case, the optical response of an LET is governed by the picosecond-range carrier transit time instead of nanosecond-range recombination lifetime.

3.4 High-Speed Light-Emitting Transistors

The optical response of LETs and QWLETs mentioned previously are limited by the parasitic resistance and capacitance and the lack of light extracting features in the material structures and the layout design in HBTs. To push an LET's performance toward its intrinsic potential, a high Al composition AlGaAs layer is included for current confinement with oxide, and a thick collector layer and common-collector configuration layout design to reduce the parasitic capacitances [3]. The epitaxial layers of the LET in Ref. [3] include a bottom cladding structure that consists of an n-type GaAs buffer layer, n-type $Al_{0.3}Ga_{0.7}As$ layer, graded Al-composition oxide buffer layer, n-type $Al_{0.98}Ga_{0.02}As$ oxidizable layer, and another oxide buffer layer. Following the bottom cladding, the following are grown: an n-type GaAs subcollector layer for contact, GaAs collector, heavily doped p-type AlGaAs/GaAs composition-graded base layer with two undoped InGaAs quantum wells designed for emission wavelength of 980nm, and then the upper cladding structure consisting of an n-type InGaP emitter, AlGaAs oxide buffer layer, a n-type $Al_{0.98}Ga_{0.02}As$ oxidizable layer, another oxide buffer layer, and an n-type $Al_{0.3}Ga_{0.7}As$ layer. Finally, the upper cladding structure is capped with a heavily doped n-type GaAs layer for emitter contact [3]. The reason for using a heavily doped subcollector and a top capping layer for contact instead of directly depositing metal onto

the actual collector and emitter is to maintain low junction capacitances at the base-collector and emitter-base junctions with lightly doped collector and emitter. Figure 8 shows the device cross section and top view of an LET with common-collector design. The oxidation process creates an oxide aperture about 6μm for current confinement and light extraction on the 10μm emitter mesas .

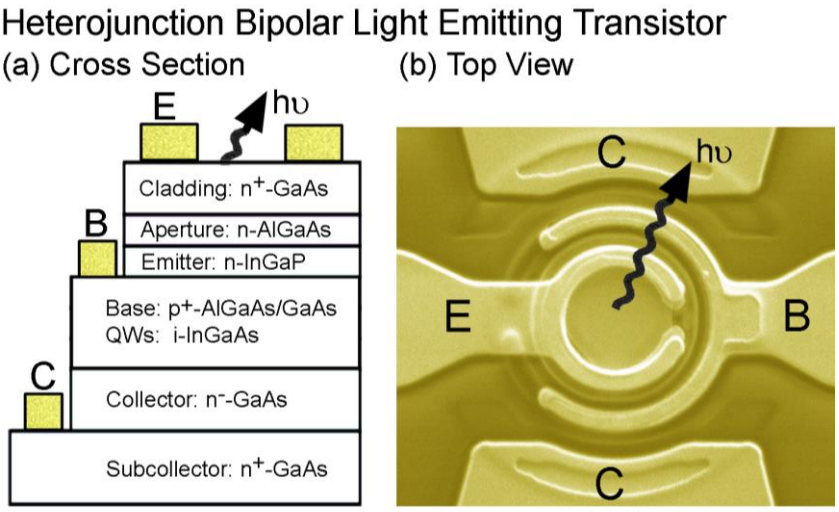

Figure 8. (a) The device cross section and (b) top view of the common-collector layout design of an LET [3]

Figure 9 shows the I-V characteristics at the collector and optical output measurement of the work reported in Ref. [3]. The LET shows a current gain β ($=\Delta I_C/\Delta I_B$) as high as 30. Note that a current gain of an LET is much lower than the current gain of an HBT because a large number of electrons in the base recombine for spontaneous emission, and the collector current decreases. The output light is collected by a large-area photodetector from the bottom of the device. The inset of Figure 9 (b) shows the emission spectrum of the device, and a full width at half maximum of 76nm indicates the spontaneous emission of an LET.

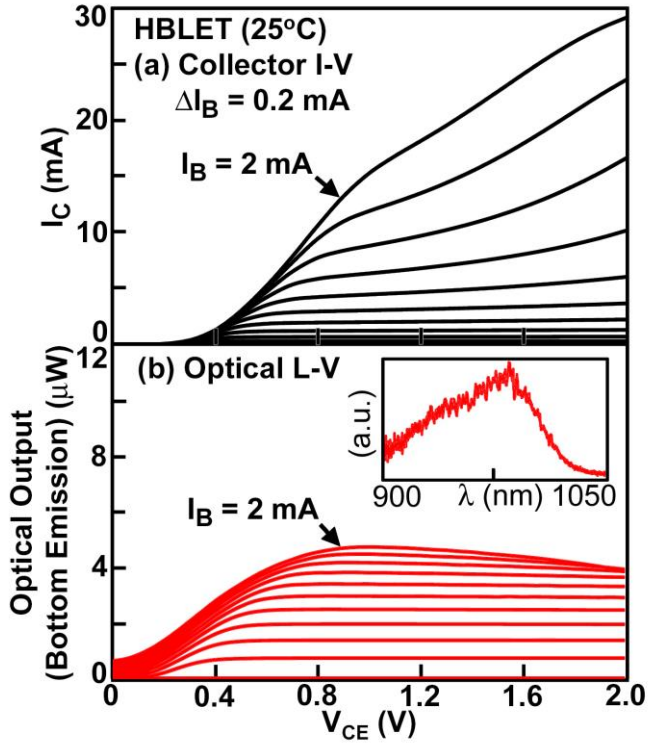

Figure 9. (a) Collector I-V characteristics and (b) optical L-V and spectrum (inset) at I_B = 2mA, V_{CE}=1.8V, and $V_{BC} \approx 0$ V [3]

In the common-collector configuration, the base-collector (BC) and the emitter-collector (EC) ports can both be used as the RF signal input port depending on the needs of the applications. Using BC port as signal input allows optical output and electrical output gain at the EC port at the same time. On the other hand, using EC port as the input does not provide gain to the electrical output at BC port, but EC port has lower input impedance for better RF signal impedance match. The BC port exhibits higher input impedance because of the reverse-biased BC junction, and it is useful when high input impedance is required. Figure 10 shows the optical response of the common-collector LET using EC and BC as input ports with I_B = 2mA and the external $V_{BC} \sim$ 0V but still

keeping the BC junction reverse-biased internally. The optical responses of the LET under two input configurations show the same -3dB modulation bandwidth of 4.3 GHz.

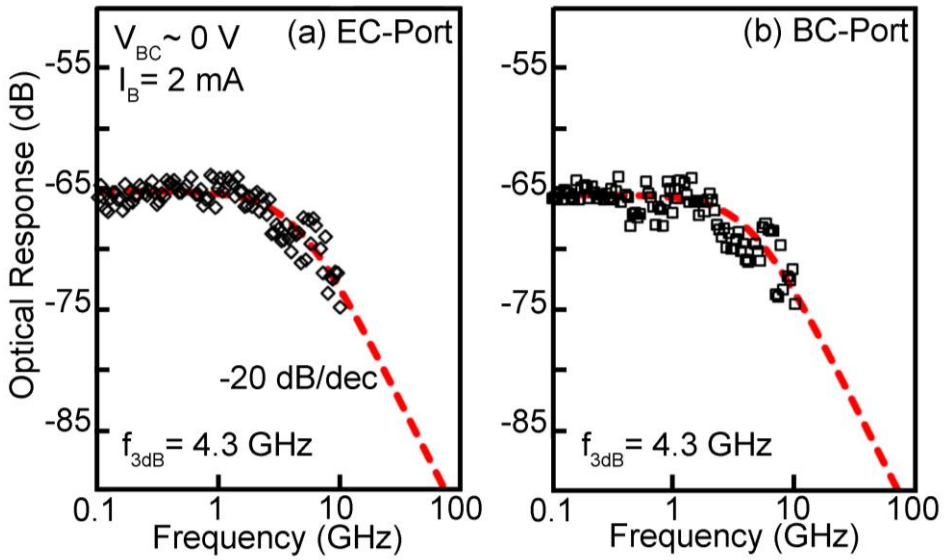

Figure 10. Optical response of the common-collector LET using (a) EC and (b) BC as input port [3]

The optical response as a function of frequency, H(*f*), can be expressed as in Equation 4.1. A_o is the electrical-to-optical efficiency, and f_{-3dB} is the frequency at which the optical response drops 3dB. From the measurement results shown in Figure 10, the f_{-3dB} of the LET is 4.3 GHz [3].

$$H(f) = \frac{A_o}{1 + j\frac{f}{f_{-3dB}}} \tag{4.1}$$

Then, the -3dB bandwidth, f_{-3dB}, can be related to the effective carrier lifetime in the base, τ_B, as shown in Equation 4.2. A 4.3GHz bandwidth is equivalent to a 37 picosecond effective base recombination life time.

$$f_{-3dB} = \frac{1}{2\pi\tau_B} \tag{4.2}$$

Recombination lifetime in the sub-100 picosecond range has not been demonstrated in an LED. An LET has inherited the advantage of having a third terminal, the collector, from an HBT. Due to the reverse bias imposed at the BC junction, the minority carrier density at the edge of the depletion region is close to zero, and the tilted charge distribution is created in the base. The large built-in field at the BC junction depletes the carriers in the base that do not recombine radiatively, so the optical response of an LET is governed by the carrier transit time, τ_t, as shown in Equation 4.3 with the diffusion coefficient, D, about 26 cm^2/s and the effective base width, W_B, of 1358 Å for the device reported [3].

$$\tau_t = \frac{W_B^2}{2D} \tag{4.3}$$

The calculated carrier transit time is 3.6 ps, so the intrinsic recombination lifetime of the carriers in the base should be of the same order. However, the effective carrier lifetime calculated from the measured bandwidth is 37 ps, about 10X larger than the transit time. It is the parasitic RC charging time that limits the speed of optical response. Further improvements in the fabrication process and layout design to reduce the parasitic capacitance and resistance can push the device toward its intrinsic limit [3].

3.5 Lateral Scaling of Light-Emitting Transistors

The effect of the oxide aperture size scaling on device's electrical and optical performances is studied in Ref. [9]. Devices with different lateral oxide aperture diameters are fabricated and compared. As scaling down the aperture diameter, the device shows higher current gain due to increased current density. However, reducing aperture diameter also leads to less area for radiative recombination, so the optical output intensity drops for LETs with smaller apertures as shown in Figure 11. Because of the circular geometry of the LETs, the fraction of the radiative recombination that truly occurs in the intrinsic base region is inversely proportional of the aperture diameter, D_A. With reduction in diameter sizes, more carriers are confined in the intrinsic base, and larger current density and higher β are shown. On the other hand, larger aperture diameters increase the contribution of carriers to both radiative and nonradiative recombination in the extrinsic base and lead to a stronger optical output with lower current gain. Figure 12 shows the optical response of LETs with different oxide aperture diameters with external V_{BC} =0 V and EC as the RF signal input port for impedance match. As seen in Figure 12, the maximum 3dB bandwidth improves from 1.8GHz to 4.3 GHz with reduction in the aperture diameter. Devices with smaller aperture diameters achieve higher bandwidths because, as mentioned, the fraction of radiative recombination occurring in the intrinsic base region, where recombination lifetime of carriers is shorter, is inversely proportional to D_A. Also, the recombination in the extrinsic base has an effect similar to parasitic capacitance and resistance and limits the bandwidths, so smaller aperture diameters can direct the carriers to the intrinsic base region and improve optical response [9].

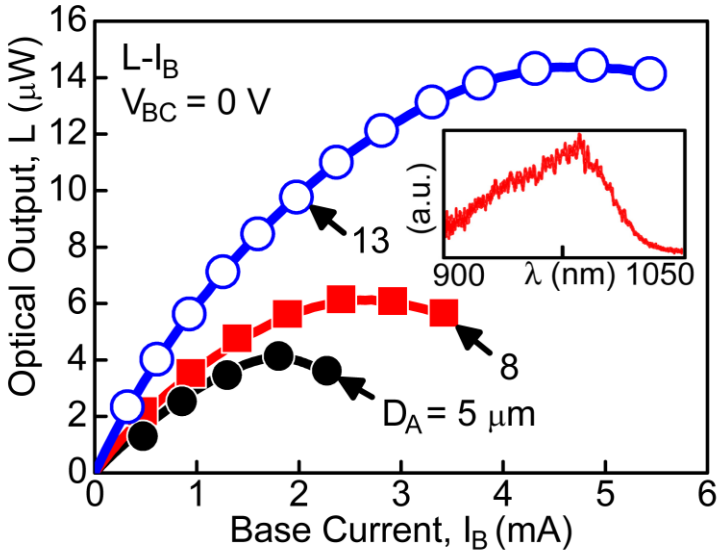

Figure 11. Optical output L-I measurements of LETs with lateral oxide aperture diameters, D_A=13,8, and 5 μm, biased under V_{BC} = 0 [9]

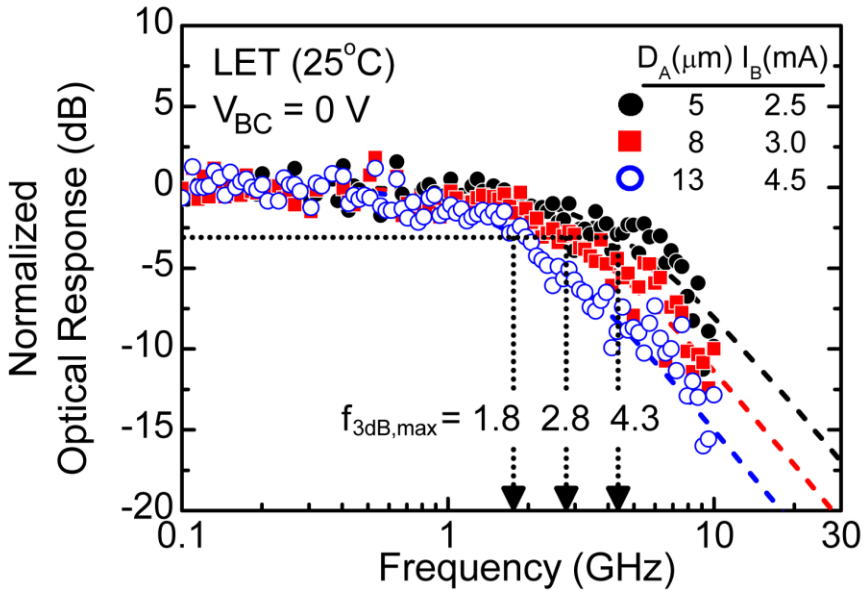

Figure 12. The maximum optical response of LETs with lateral oxide aperture diameters, D_A=13,8, and 5 μm, biased under V_{BC} = 0 and EC as RF input [9]

3.6 Tilted-Charge Light-Emitting Diode

As mentioned in the previous sections, LETs are capable of achieving high modulation bandwidths due to the advantage of the third terminal, the collector, to filter out the carriers that cannot recombine within the base transit time. By using the collector to drain out the slow carriers, a new kind of LED, the tilted-charge LED, is demonstrated in Ref. [10]. Figure 13 shows the cross section of a tilted-charge LED; the n-p diode configuration is formed at the emitter-base diode. As in an LET case, the carriers are injected from the emitter to collector, or, in the tilted-charge LED case, the drain. Some carriers recombine radiatively in the active region and others form the drain current. The reverse built-in field at the base-drain junction is maintained by a common contact metal extending from base to drain. The zero external potential difference between the base and the drain ensures the tilted charge distribution in the base [10].

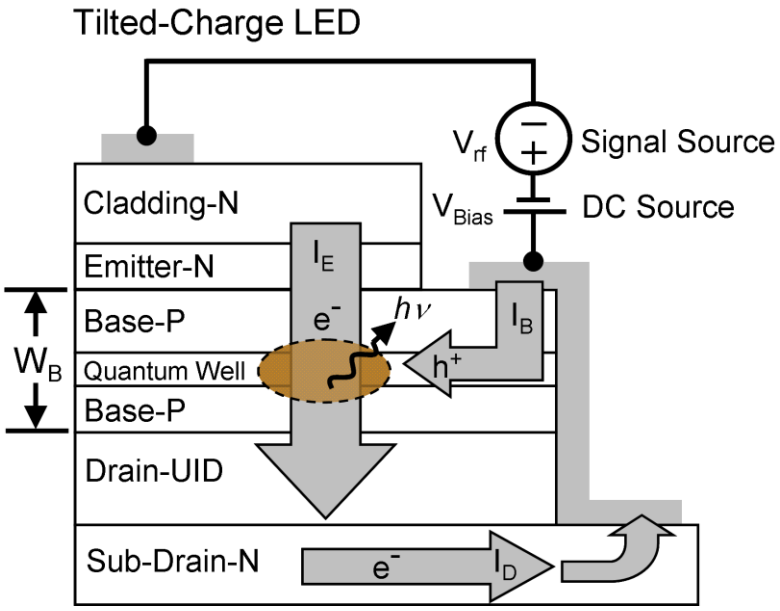

Figure 13. Cross section of the tilted-charge LED with the active quantum well region in the base [10]

The 2-terminal tilted-charge LED is biased as a conventional LED. The diode I-V curve is shown in Figure 14, and the diode turn-on voltage is determined by the potential difference between the emitter and the base [10]. The inset of Figure 14 is a SEM image of the device showing the 2-port configuration.

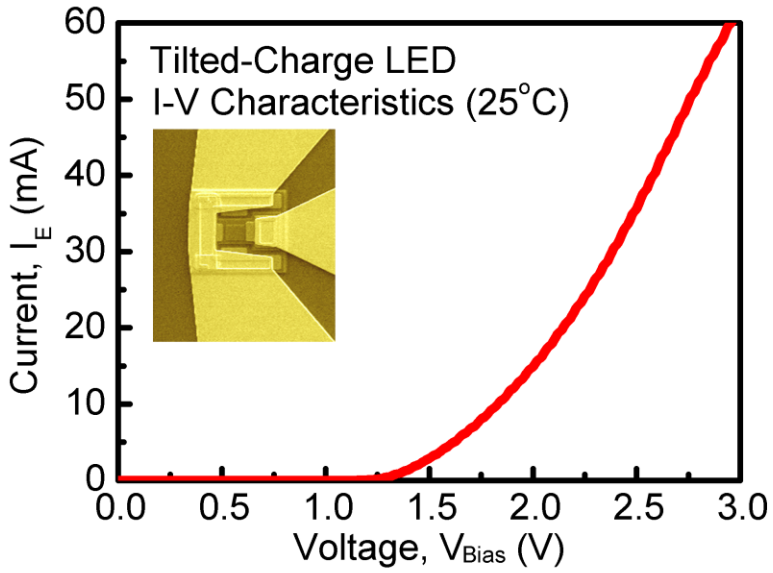

Figure 14. The I-V characteristic of the tilted-charge LED, and inset is the SEM image of the device [10]

Figure 15 shows the optical response of a tilted-charge LED at different emitter input currents. As the emitter current is increased from 40 mA to 60mA, the -3dB bandwidth improves from 3.2 GHz to 7 GHz. Due to the drain layer, the tilted-charge LED can be modulated much faster than a conventional LED can. Previously, the high-speed LET in Ref. [3] shows a -3dB bandwidth of 4.3 GHz because the parasitic RC-charging time limits the optical response. In the layout design of tilted-charge LED, the original ring-like feeding structure in the LET is changed to lateral feeding as shown in Figure 16. The lateral extrinsic resistance, R_{cir}, of the device in Ref.3 with the ring-like

geometry can be calculated as in Equation 4.4, where R_{sh} is the base sheet resistance, r_B is the radius of base contact, and D_A is the radius of the oxide aperture [11]. As D_A is decreased for faster optical response [3], the resistance also increases and limits the speed of device.

$$R_{cir} = \frac{R_{sh}}{2\pi}\ln\left(\frac{r_B}{D_A/2}\right) \tag{4.4}$$

The lateral extrinsic resistance, R_{lat}, of the lateral feeding geometry, as shown in Figure 16 (b), in a tilted-charge LED is expressed in Equation 4.5, where L is the emitter width, d is the distance between base contact and emitter mesa, and t is the intrinsic device width measured from the emitter mesa edge (t < W) [11].

$$R_{lat} = R_{sh} \times \frac{(d+t)}{L} \tag{4.5}$$

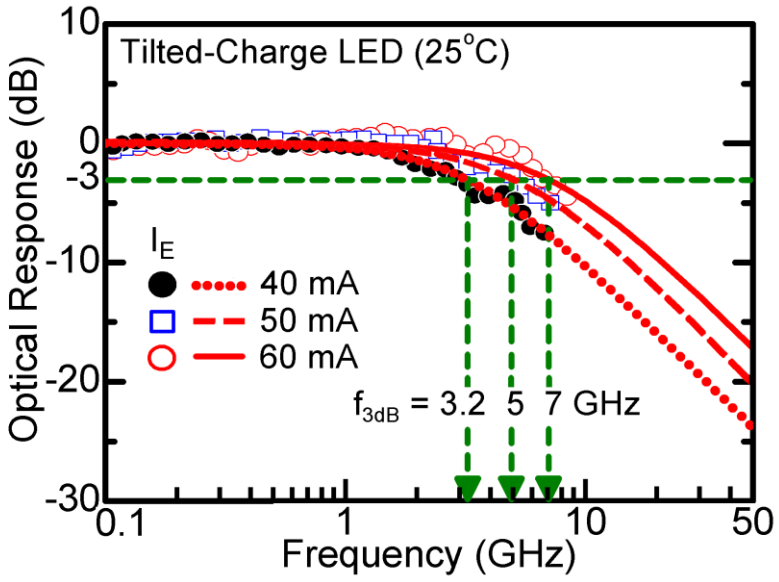

Figure 15. The optical response of the tilted-charge LED at bias currents I_E = 40, 50, and 60 mA [10]

With W=5μm and t =1μm, R_{lat} can be reduced with increasing L. However, larger L, i.e. larger emitter, also causes large capacitance. With optimized L=10μm, the maximum optical modulation bandwidth of 7GHz is achieved in a tilted-charge LED [10].

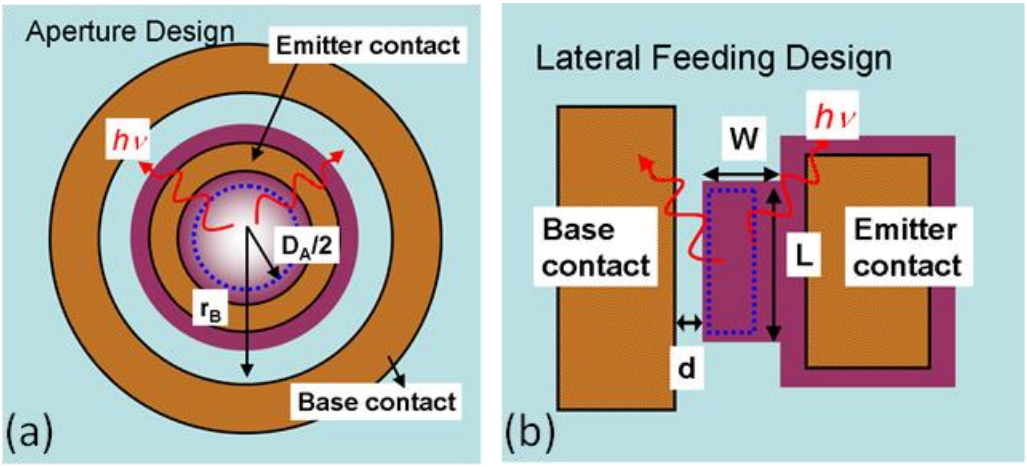

Figure 16. (a) The ring-like feeding geometry in a LET, and (b) the lateral feeding design in the tilted-charge LED [11]

Chapter 4: Resonant Cavity Light-Emitting Transistors

4.1 Resonant Cavity

In optical communication applications, besides modulation speed, the light output intensity and the spectral purity of the optical signal are also important. A resonant cavity structure is introduced into a light-emitting transistor to improve the emission intensity and spectral purity. A resonant cavity is formed by placing the LET structure between top and bottom mirrors. The mirrors are made of distributed Bragg reflectors (DBRs), i.e. alternating high- and low-refractive-index material layers. One pair of DBR is defined as combination of one low index layer and one high index layer, and each layer is a quarter-wavelength thick. A mirror made of more pairs of DBRs has a higher reflectivity, and theoretically as the number of pairs reaches infinity, the reflectivity of the mirror approaches 1. Due to a finite reflectivity of DBRs, light is extracted from the less reflective mirror. The light from radiative recombination in the active region is reflected by the top and bottom mirrors in a cavity, and the cavity length is designed so that the light can form a standing-wave pattern. The cavity length is multiples of half wavelengths, and only the resonant light can from a standing wave. The off-resonant emission is suppressed by the cavity, and the spectral purity of a resonant cavity light-emitting transistor (RCLET) is improved when compared with a conventional LET. Higher purity of the emission spectrum can reduce the chromatic dispersion while light is guided in the optical fiber. To increase the emission intensity, the active region is designed to be at the antinode of the stand wave, so the maximum gain-intensity product

is achieved. Also, the wavelength of the light from the quantum wells may shift due to the rise of temperature while in operation. However, with a resonant cavity, the wavelength shift with temperature of the emission light from a RCLET is determined by the temperature sensitivity of the resonant cavity, which is much less than the temperature sensitivity of material band gap, so the temperature stability of a RCLET is higher than a conventional LET [12].

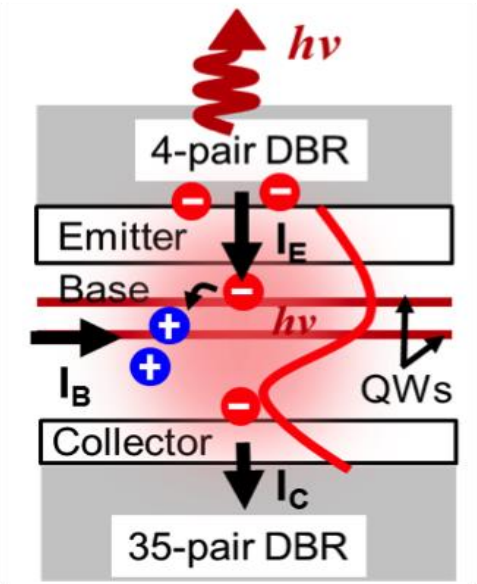

Figure 17. Cross section and the current flows of the RCLET with cavity designed to be one wavelength of the 980nm emission light from the quantum wells

Figure 17 is the illustration of the cross section of a RCLET and the current flows inside the device. The conventional LET structure is sandwiched between the top and bottom DBR mirrors. Electrons are injected by the emitter current (I_E) from the emitter to the base. Electrons and holes recombine in the quantum wells in the base, and the electrons that do not recombine are swept to the collector to form the collector current. The loss of hole population due to recombination is resupplied by the base current (I_B).

Top and bottom mirrors are made to 4 and 35 pairs of DBRs. The less reflective top mirror is for light extraction. The cavity length is one full wavelength of 980nm emission light from the quantum wells in the base, and the quantum wells are aligned with the antinode of the standing wave for maximum gain in the intensity. In addition, since standing wave is formed along the optical axis, which is normal to the light-extracting surface, the emission light of a RCLET is more directional, and higher coupling efficiency into the optical fiber or waveguide can be achieved [12].

4.2 Fabrication of Resonant Cavity Light-Emitting Transistors

The material structure of the RCLET consists of a bottom mirror made of 35 pairs of $Al_{0.12}Ga_{0.88}As/Al_{0.9}Ga_{0.1}As$ DBRs. On top of the bottom mirror are a 200Å n^+-GaAs sub-collector and a 1000Å intrinsic $Al_{0.12}Ga_{0.88}As$ collector. The collector is undoped, and the sub-collector is used for metal contact to reduce the base-collector junction capacitance while maintaining a good ohmic contact. The base is made of an 1100Å p^+-$Al_{0.05}Ga_{0.95}As$ layer with 2 undoped $In_{0.2}Ga_{0.8}As$ quantum wells included. Following the base, a 500Å n-$In_{0.49}Ga_{0.51}P$ layer is grown as the wide-gap emitter. Resonant cavity is formed with the top mirror made of 4 pairs of $Al_{0.12}Ga_{0.88}As/Al_{0.9}Ga_{0.1}As$ DBRs. For the top n-type contact, an n^+-GaAs cap layer is grown to complete the RCLET structure [4].

To fabricate a RCLET, there are 6 photolithography steps and 8 processing steps : 1 inductively coupled plasma (ICP) reactive ion etch (RIE) or a wet etching step, 2 wet etching steps, 3 metal depositions, 1 via hole opening step, and 1 metal interconnect deposition. To etch the emitter contact cap layer and top DBR mirror, ICP RIE or wet

etching can be used. For ICP RIE, a SiN_x hard mask is first deposited by STS PECVD on top of the contact cap layer. Then the SiN_X hard mask is defined by photolithography and the etched by reactive ion etch (RIE) using CF_4 plasma. After the SiN_X hard mask is patterned, the photoresist mask used for RIE is removed by acetone, and the sample is ready for ICP RIE. $SiCl_4$ plasma is used in ICP RIE to etch the top contact cap and the top mirror. The ICP RIE can be controlled to stop at the InGaP emitter because the etching rate of InGaP in $SiCl_4$ plasma is about one quarter that of AlGaAs. Figure 18 (a) shows the cross section of the sample after ICP RIE. Sulfuric-acid-based solution, H_2SO_4:H_2O_2:H_2O=0.5:5:100, can also etch the top DBRs, and the etching can stop at InGaP emitter due to selectivity. Photoresist instead of SiN_x is used as the etching mask in wet etching. After the emitter etch is done by ICP RIE or wet etch, the sample is sent into a furnace filled with water vapor for a shallow oxidation to seal the sidewall of the top mirror. This step is critical to protect the top DBRs in the following wet etching steps in the device fabrication. At this point, the emitter mesa is created and the emitter layer is exposed. The SiN_x hard mask is removed by RIE and InGaP emitter is then removed with hydrochloric acid to expose the base layer for contact as shown in Figure 18 (b). To create the base mesa, a photolithography step is used to pattern the photoresist as the etching mask, and then the base and the collector are etched by 10:1 citric acid to hydrogen preoxide (H_2O_2) solution. After the base/collector etch, the sub-collector layer is exposed for metal contact, and the device cross section is shown in Figure 18(c). After all the contact layers are exposed, a last wet etching step, the isolation etch, is performed to isolate the RCLETs. Again, a photoresist etching mask is defined by lithography, and

the bottom DBRs are etched by H_2SO_4:H_2O_2:H_2O=0.5:5:100 solution. Isolation etch is used to prevent signal leakage when RCLETs are in RF operation. Ti/Pt/Au contact metal is then deposited using electron-beam evaporator as the for p-type base. Titanium is used as an adhesion metal to ensure good interface between the semiconductor and metal, platinum serves as a blocking layer to prevent gold diffusing into the semiconductor, and gold is the actual contact metal. AuGe/Ni/Au is then deposited as n-type emitter and collector contact metal. To improve n-type ohmic contacts, the sample is annealed in a nitrogen furnace at 325℃ to alloy AuGe. Nickel is the wetting layer between gold-germanium alloy and gold. The device cross section after metal depositions is shown in Figure 18(d). Polyimide is then spin-coated onto the sample and cured at high temperatures for device passivation. For metal interconnect, SiNx is again defined by photolithography and RIE to serve as the etching mask for via opening, and then polyimide is etched by RIE using oxygen plasma to open via. After via is opened, as shown in Figure 18 (e), interconnect metal, Ti/Au, is deposited using e-beam evaporator, and the cross section of a complete device is shown in Figure 18 (f).

Figure 19 shows the scanning electron microscope (SEM) image of a RCLET. The carriers are fed into the active region laterally from the emitter, and the cavity is between the emitter metal and the base metal. Collector metals on the sides show that the device is designed for common-collector configuration. The isolation is created by etching away the bottom DBRs to separate the neighboring RCLETs so the RF signal leakage can be reduced to minimize the parasitic capacitance.

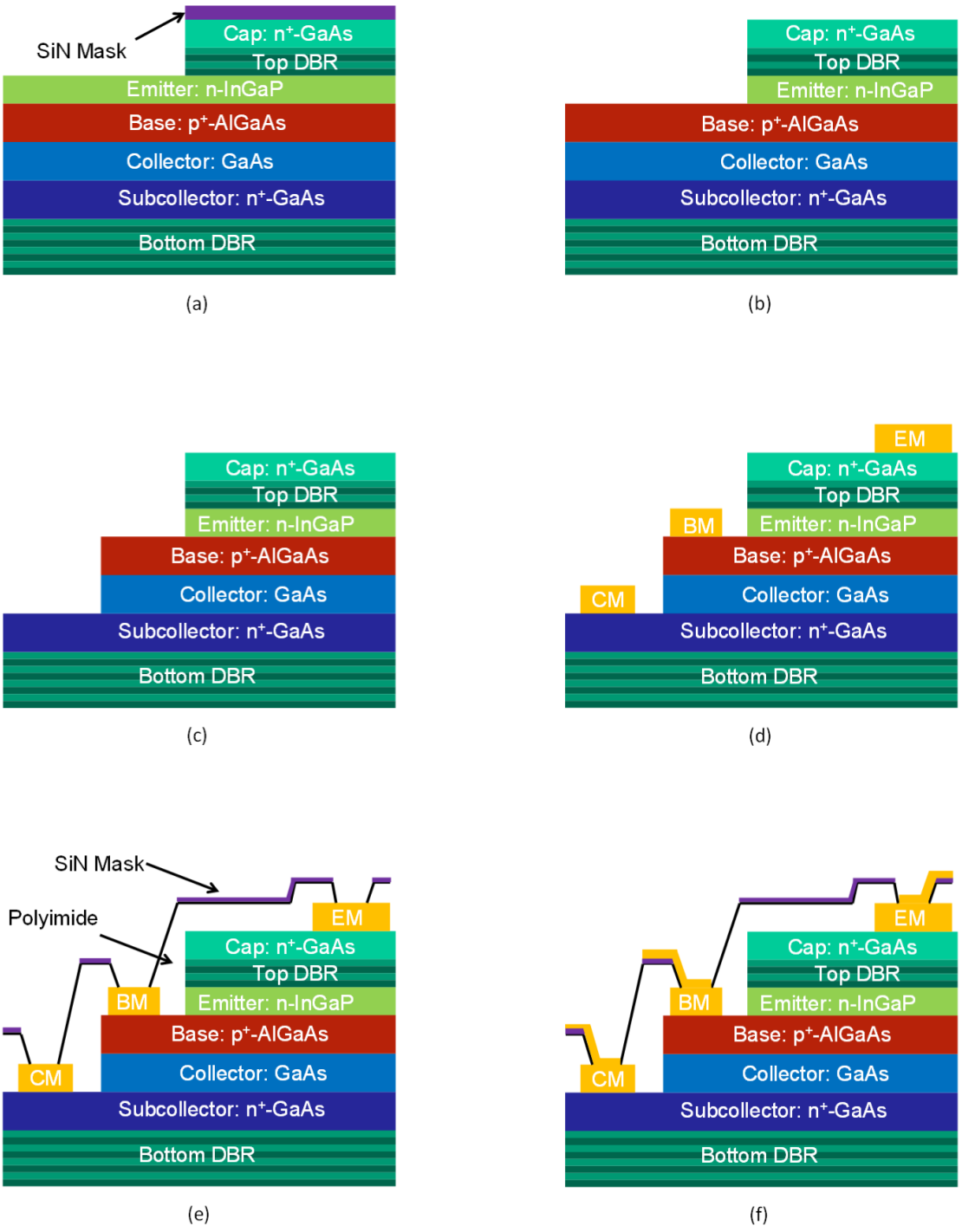

Figure 18. Device cross sections (a) after ICP RIE emitter/top DBR etch, (b) after SiN_x removed by RIE using CF_4 plasma and InGaP emitter etched by HCl, (c) after base/collector etch using citric acid, (d) after contact metal deposition, (e) after via opening using SiN_x mask and oxygen plasma, and (f) a finished RCLET

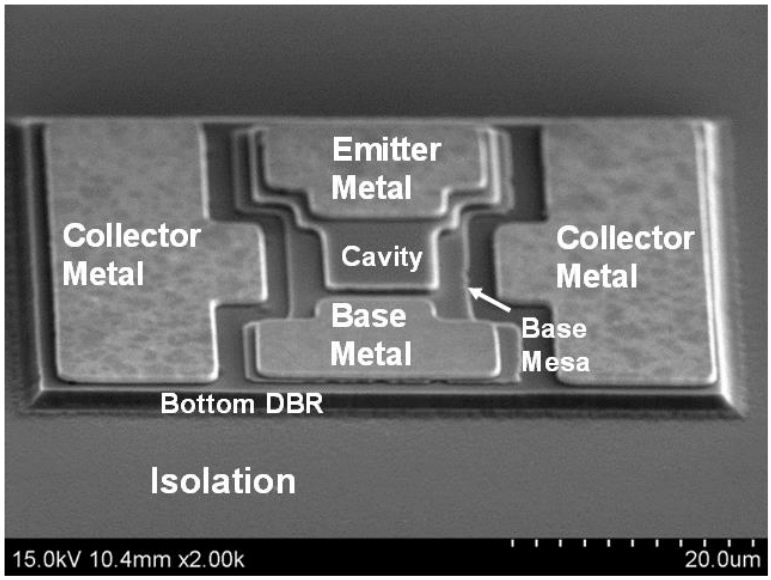

Figure 19. The scanning electron microscope (SEM) image of a common-collector RCLET

4.3 Characterization of Resonant Cavity Light-Emitting Transistors

Figure 20 shows the spectra of a RCLET and a conventional LET [4]. The setup for spectrum measurement is shown in Figure 21. Device is biased by a modular DC source through bias tees and GSG probes in common-collector configuration, and the emission light is collected by a multimode optical fiber probe. The coupled light is then sent into an optical spectrum analyzer. The full width at half maximum (FWHM) of a conventional LET's spectrum is 96nm, and a RCLET's spectrum shows a FWHM of 16nm. By inserting a resonant cavity structure into an LET, the 980nm spontaneous emission light from the InGaAs quantum wells in the base is enhanced, and the off-resonant light is suppressed. The higher spectral purity of a RCLET can reduce the chromatic dispersion during light transmission in optical communication applications.

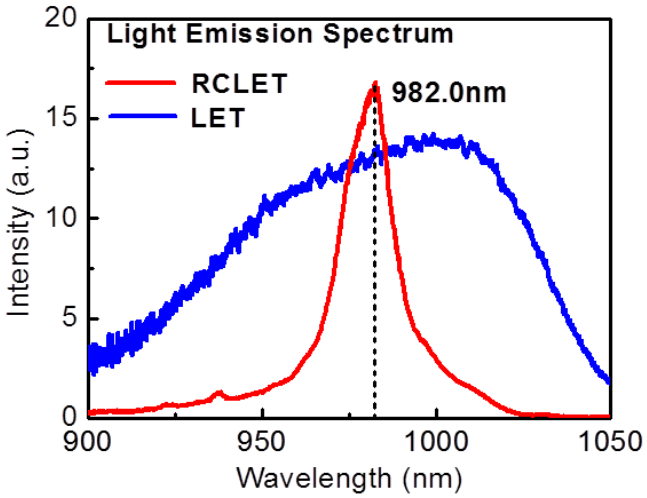

Figure 20. Emission spectra of a conventional LET and a RCLET [4]

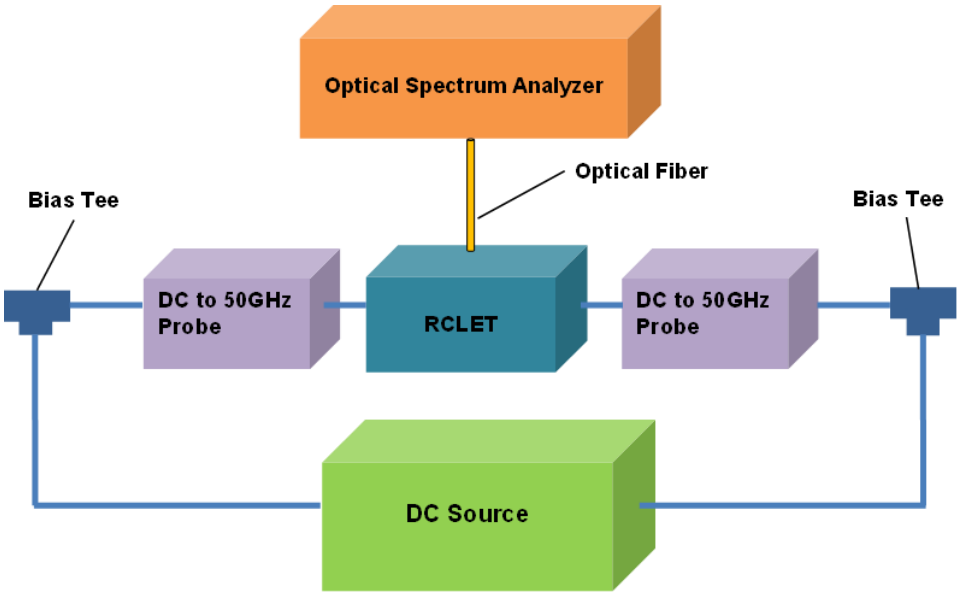

Figure 21. The setup of spectrum measurement: device is biased by a DC source through bias tees and GSG probes; the output light is collected by multimode optical fiber and sent into an optical spectrum analyzer

The sidewall profile of the etched top mirror can affect the scattering of light while light is extracted from the less reflective top mirror. Figure 22 shows the sidewall profiles of the top DBR mirrors in RCLETs etched by (a) ICP RIE and (b) sulfuric acid. The top DBRs etched by ICP RIE show a much smoother sidewall profile. ICP can be

operated at low pressure and can achieve high plasma density, so the etching process is more anisotropic, and a straight sidewall can be created. On the other hand, a chemical etch is isotropic, so material is etched both vertically and horizontally at the same time. Also, the high and low index layers of DBRs show different etching rates due to the difference in aluminum composition. An isotropic etching process and the difference in etching rates cause a wavy sidewall for the top mirror etched by sulfuric acid.

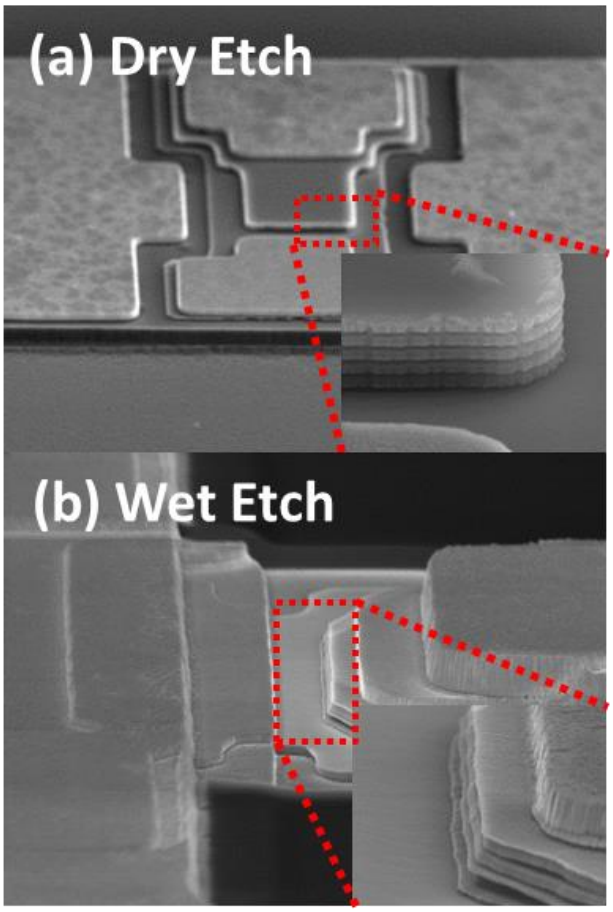

Figure 22. The SEM images of RCLETs' top mirror sidewall etched by (a) ICP RIE and (b) wet etch [4]

Figure 23 shows the emission intensity as a function of emitter current of RCLETs with top DBRs etched by dry ICP RIE and wet etch and a conventional LET,

and all the devices have emission areas of 10x10 μm^2. The RCLET with top DBRs etched by sulfuric acid shows a peak intensity of 1.6μW compared with a conventional LET's peak intensity of 0.7μW, and the RCLET with dry ICP etched top DBRs has a peak intensity of 2.7μW, about 4x enhancement. Also, the dry-etched RCLET shows a larger roll-off current of 30mA compared with the 17mA roll-off current of a conventional LET. The roll-off current is the point at which the increase in emitter current causes the luminescence intensity to drop due to saturation and heating. Both enhanced emission intensity and a larger roll-off current indicate more radiative recombination in a dry-etched RCLET [4].

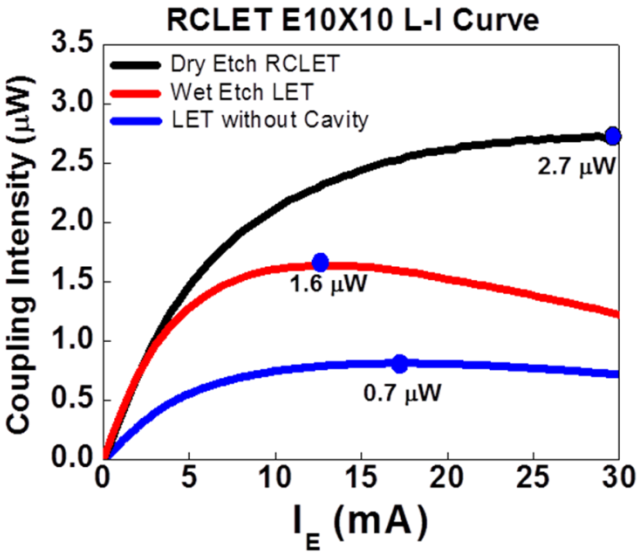

Figure 23. Emission intensity as a function of emitter current of a conventional LET and RCLETs with top mirror etched by dry ICP etch or wet etch [4]

In an LET and a RCLET, the carriers that do not recombine in the base are swept to the collector to from collector current, so the electrical data can also indicate the increase in emission intensity in the RCLETs. As shown in Figure 23, a dry-etched

RCLET shows a larger emission intensity compared with a wet-etched RCLET. Figure 24 shows the electrical family curves of the two kinds of RCLETs both with a 10x10 μm^2 emission area. The wet-etched device shows a current gain, β, of 2.14 at 5mA base current, and the dry-etched device exhibits a β of 1.418 [4]. The reduction in the current gain indicates more recombination in the base and stronger optical output intensity. As mentioned in Section 3.2, the radiative recombination in an LET occurs at the emitter-base junction [2], and the RCLET has a lateral feeding geometry, so the radiative recombination occurs along the peripheral of the emitter mesa. Thus, the scattering of light at the sidewall of a RCLET plays an important role in optical output intensity [4]. Both optical and electrical data show that the smoother sidewall achieved by ICP RIE leads to a better cavity quality and a stronger light output.

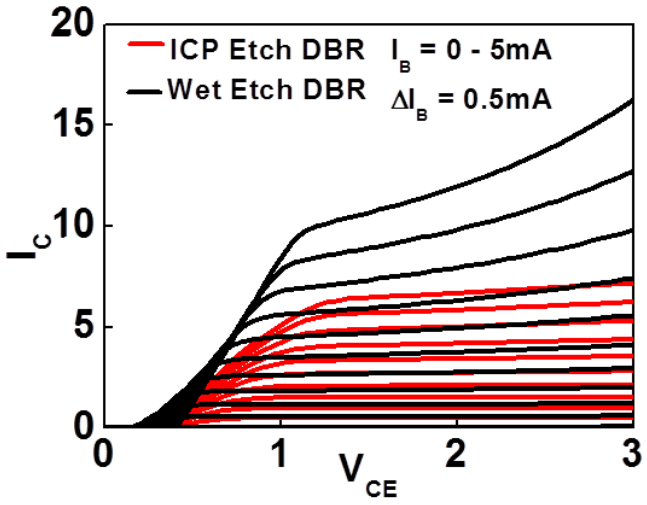

Figure 24.The common-collector family curves of wet-etched and dry-etched RCLETs [4]

Figure 25 shows the setup for optical response measurement. The DC bias is provided by a modular DC source, and the RF signal comes from a parameter network analyzer (PNA). The DC and RF signals are combined by bias tees and sent to GSG

probes which can take RF signal up to 50 GHz. A RCLET is probed in common-collector configuration, and the optical output is collected by a multimode optical fiber probe and sent to a photodetector. A photodetector converts an optical input to an electrical output, and the electrical signal is amplified by an amplifier, then sent into a PNA to see the frequency response.

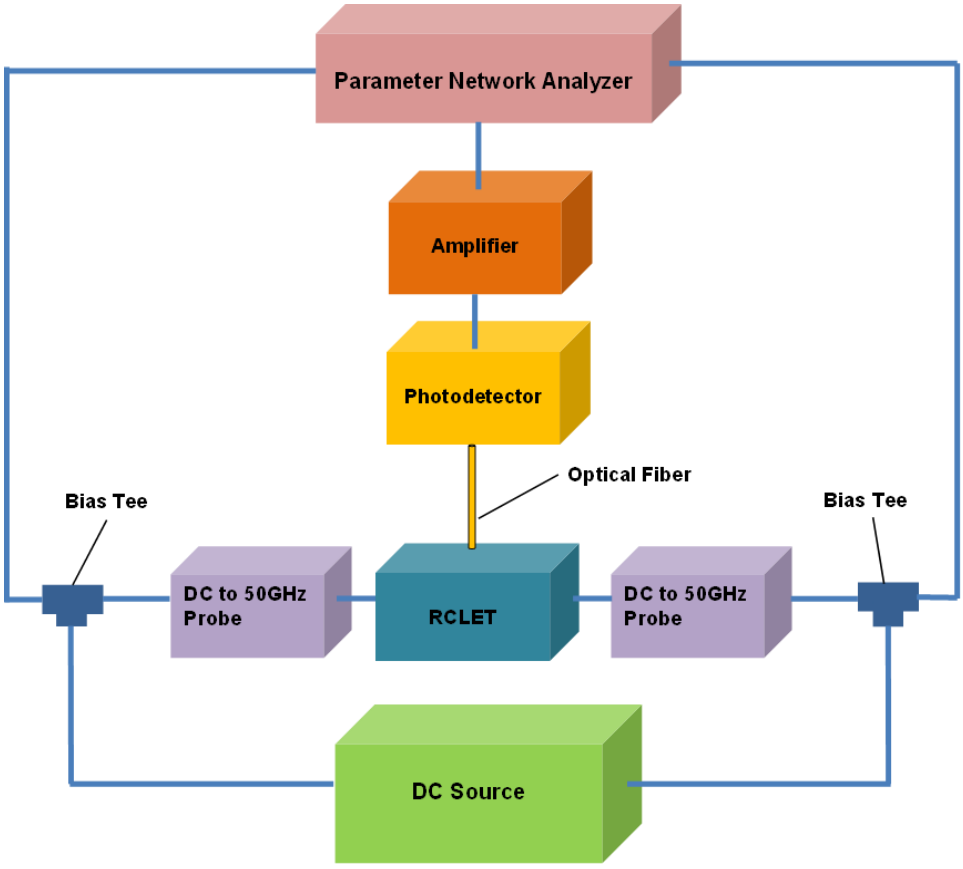

Figure 25. The equipment setup for optical response measurement: bias DC and RF signal are sent to a RCLET through bias tees and GSG probes; the output light is collected by multimode optical fiber and converted to electrical signal by a photodetector; and the amplified electrical signal is sent into a PNA

Figure 26 shows the optical response of a RCLET with $10x3\mu m^2$ emission area in base-collector-shorted configuration at 15^oC. The -3dB bandwidth of the device is 2.3GHz at 30mA emitter current. Although further increase in the emitter current will

degrade the optical output intensity due to saturation and heating, the -3dB bandwidth can be pushed to 4GHz at 60mA emitter current [4].

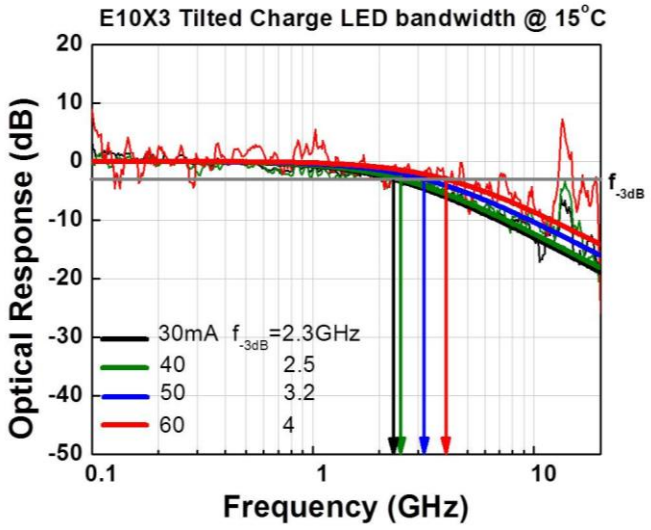

Figure 26. The optical response of a 10x3μm^2 RCLET in base-collector-short bias configuration [4]

With a resonant cavity in an LET, a RCLET can achieve higher optical output intensity and spectral purity. A resonant cavity suppresses the off-resonant emission and supports a standing wave pattern for the desired emission wavelength, and thus the spectral purity is improved. Further, by aligning the quantum wells with the antinode of the standing wave formed in the cavity, the light output intensity is enhanced. The smoothness of the sidewall of the etched top DBRs can affect the quality of a cavity. The improvement in optical output due to reduced scattering from a smooth sidewall can be proved by both optical and electrical data.

Chapter 5: Conclusion

LETs have demonstrated high-speed modulation capability because of their dynamic charge transport in the base. The injected electrons from the emitter show a tilted charge distribution in the base, and the electrons diffuse toward collector based on the concentration gradient. To enhance radiative recombination, quantum wells are inserted into the base for carrier confinement. While transporting through the base, the electrons pass the quantum wells, and those electrons that do not recombine radiatively within the base transit time are swept to the collector and form collector current. Compared with a p-i-n LED, the carriers in the base of an LET do not pile up, so the optical response is not limited by the nanosecond recombination lifetime. Because of the reverse bias imposed at the base-collector junction, the collector serves as a filter for the carriers that cannot recombine within the base transit time; thus, in an LET, the optical response is governed by the picosecond range carrier transit time.

To further improve the device performance for optical communication applications, a resonant cavity is introduced into an LET to enhance the optical output intensity and spectral purity. A resonant cavity can suppress the off-resonant emission and support the light of desired wavelength to form a standing wave in the cavity, so the spectral purity is improved. By further aligning the quantum wells with the antinode of the standing wave, the output intensity is enhanced.

References

[1] M. Feng, N. Holonyak, Jr., and W. Hafez, "Light-emitting transistor: Light emission from InGaP/GaAs heterojunction bipolar transistors," *Applied Physics Letters*, vol. 84, no. 1, pp. 151-153, 2004.

[2] M. Feng, N. Holonyak, Jr., and R. Chan, "Quantum-well-base heterojunction bipolar light-emitting transistor," *Applied Physics Letters*, vol. 84, no. 11, pp. 1952-1954, 2004.

[3] G. Walter, C. H. Wu, H. W. Then, M. Feng, and N. Holonyak, Jr., "4.3 Ghz optical bandwidth light emitting transistor*," Applied Physics Letters*, vol. 94, no. 24, p. 241101, 2009.

[4] M. K. Wu, M. Liu, and M. Feng, "Improvement in spontaneous emission of resonant cavity light emitting transistors via inductively coupled plasma etching top distributed Bragg reflector," in CSMANTECH, 2013.

[5] W. Shockley, "Circuit element utilizing semiconductive material," U.S. Patent 2,569,347, Sept 25, 1951.

[6] H. Kroemer, "Theory of a wide-gap emitter for transistors," *Proceedings of the IRE*, vol. 45, no. 11, pp. 1535-1537, 1957.

[7] H. Kroemer, "Heterostructure bipolar transistors and integrated circuits," *Proceedings of the IEEE*, vol. 70, no. 1, pp. 13-25, 1982.

[8] C.H. Chen, M. Hargis, J. M. Woodall, M. R. Melloch, J. S. Reynolds, E. Yablonovitch, and W. Wang, "GHz Bandwidth GaAs Light-emitting Diodes," *Applied Physics Letters*, vol. 74, no. 21, pp. 3140-3142, 1999.

[9] C. H. Wu, G. Walter, H. W. Then, M. Feng, and J. N. Holonyak,"Scaling of Light Emitting Transistor for Multigigahertz Optical Bandwidth," *Applied Physics Letters*, vol. 94, no. 17, p. 171101, 2009.

[10] G. Walter, C. H. Wu, H. W. Then, M. Feng, and J. N. Holonyak, "Tilted-charge High Speed (7 GHz) Light Emitting Diode," *Applied Physics Letters*, vol. 94, no. 23, p.231125, 2009.

[11] C. Wu, G. Walter, H. Then, and M. Feng, "Design and Layout of Multi GHz Operation of Light Emitting Diodes," in CSMANTECH, 2010, pp.247-250.

[12] E. Schubert, *Light-Emitting Diodes*. New York, NY: Cambridge University Press, 2003, Ch. 10.